Topological Creation of Acoustic Pseudospin Multipoles in a Flow-Free Symmetry-Broken Metamaterial Lattice

Zhiwang Zhang,[1] Qi Wei,[1] Ying Cheng,[1,2,*] Ting Zhang,[1] Dajian Wu,[3] and Xiaojun Liu[1,2,†]
[1]Key Laboratory of Modern Acoustics, Department of Physics and Collaborative Innovation Center of Advanced Microstructures, Nanjing University, Nanjing 210093, China
[2]State Key Laboratory of Acoustics, Chinese Academy of Science, Beijing 100190, China
[3]School of Physics and Technology, Nanjing Normal University, Nanjing 210046, China
(Received 29 August 2016; published 23 February 2017)

The discovery of topological acoustics has revolutionized fundamental concepts of sound propagation, giving rise to strikingly unconventional acoustic edge modes immune to scattering. Because of the spinless nature of sound, the "spinlike" degree of freedom crucial to topological states in acoustic systems is commonly realized with circulating background flow or preset coupled resonator ring waveguides, which drastically increases the engineering complexity. Here we realize the acoustic pseudospin multipolar states in a simple flow-free symmetry-broken metamaterial lattice, where the clockwise (anticlockwise) sound propagation within each metamolecule emulates pseudospin down (pseudospin up). We demonstrate that tuning the strength of intermolecular coupling by simply contracting or expanding the metamolecule can induce the band inversion effect between the pseudospin dipole and quadrupole, which leads to a topological phase transition. Topologically protected edge states and reconfigurable topological one-way transmission for sound are further demonstrated. These results provide diverse routes to construct novel acoustic topological insulators with versatile applications.

DOI: 10.1103/PhysRevLett.118.084303

The discoveries of the quantum Hall effect (QHE) [1,2], quantum spin Hall effect (QSHE) [3,4], and topological insulators (TI) [5–8] have revolutionized our understanding of condensed matter physics. Their novel topological properties offer great flexibility for manipulating robust edge states and promise unprecedented functionality ranging from spintronics to quantum computation [9]. The concepts further stimulate the search for analogous states in structures supporting classical waves [10–15]. Analogous "topological photonic states" were demonstrated in photonic crystals constructed with gyromagnetic materials [16–19], bianisotropic metamaterials [20,21], and coupled waveguide networks [22–24].

These concepts have also inspired a novel field of "topological acoustics" [25–32]. However, the intrinsic difference between electrons and acoustics determines that creating the "spinlike" degree of freedom is fundamentally difficult in acoustic systems, because ordinary acoustic materials (such as air, water, etc.) only support the polarization state of longitudinal vibration and generally lack an efficient mechanism for accomplishing circulating energy flow. A promising breakthrough to tackle this problem was achieved by Khanikaev [26] and Yang *et al.* [27], who independently introduce a circulating fluid flow in the background field to break time-reversal symmetry in an acoustic system. Topological acoustic states were demonstrated in these acoustic nonreciprocal circulators based on angular-momentum bias [28,31,32], which is analogous to the strong magnetically bias in electronic graphene with QHE. Recently, decoupled acoustic pseudospins have also been demonstrated in preset coupled resonator ring waveguides under time reversal invariants [29,30], which support twofold degenerated clockwise and anticlockwise circulating modes with QSHE. The interring couplings could be specifically engineered to be aperiodic in the lattice, giving rise to a uniform effective bias field. However, such a requirement may limit their practical applicability due to the considerable fabrication complexity and the resonator lattice of several-wavelength size, which is a great technical challenge. It is more imperative to design external "force"-free topological states with a simple structure in acoustic systems.

The purpose of this work is to establish the conditions for creating the acoustic pseudospin multipolar states in a flow-free symmetry-broken metamaterial lattice. By judiciously breaking the symmetry of a regular honeycomb lattice [33] without topological properties, we build a "metamolecules" lattice with acoustic pseudospins and topologically protected states. The direction of sound propagation within each metamolecule (i.e., clockwise or anticlockwise) plays the role of pseudospin (i.e., pseudospin down or pseudospin up). Tuning the strength of intermolecular coupling by simply contracting or expanding the hexagonal packed constitutive resonators can induce band inversion between pseudospin dipole and quadrupole, which further leads to topological phase transition between nontrivial and trivial states [34,35]. Finally, topologically protected edge states and reconfigurable one-way transmission are demonstrated.

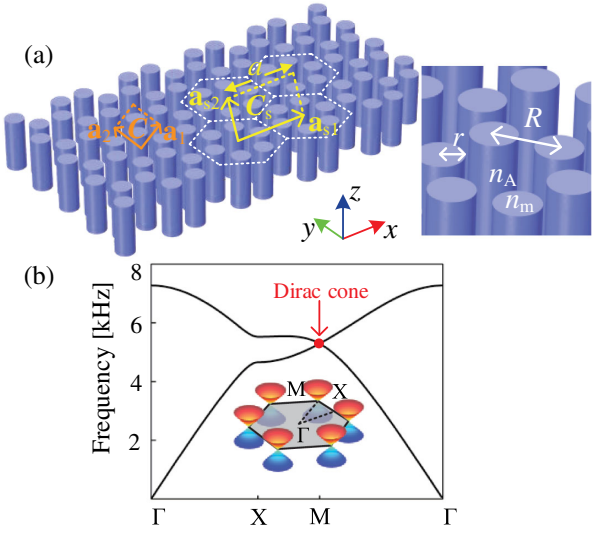

FIG. 1. (a) Schematic of the triangular acoustic metamaterial lattice composed of artificial "metamolecules." Inset: enlarged view of the metamolecule. (b) Dispersion relation of the lattice based on the original unit cell C. (Inset: single Dirac cones at the 1st BZ corners).

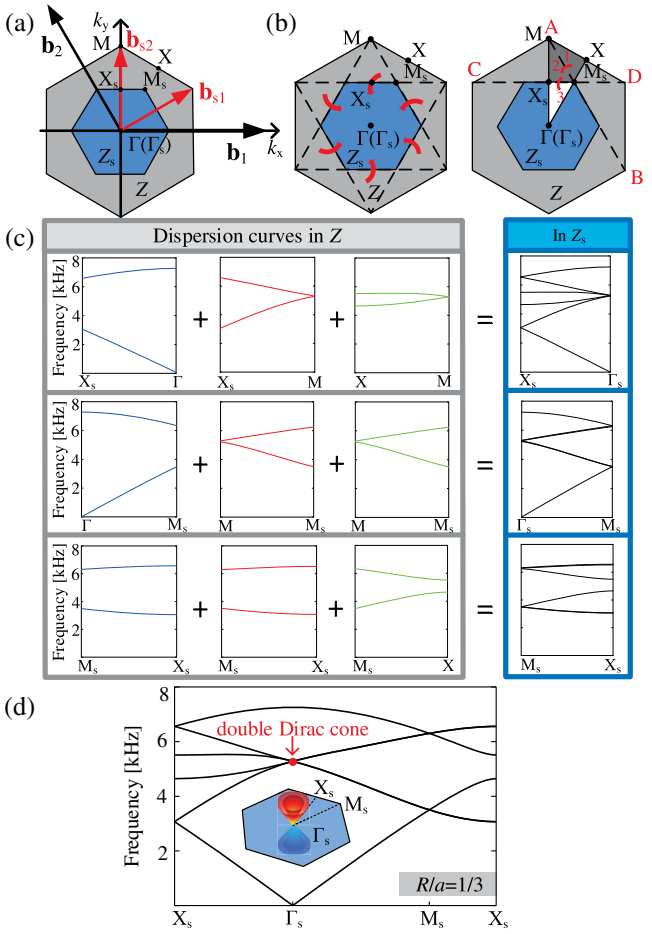

FIG. 2. (a) The 1st BZs of the original unit cell C (gray, marked as Z) and C_s (blue, marked as Z_s). ($\mathbf{b}_1$, $\mathbf{b}_2$) and ($\mathbf{b}_{s1}$, $\mathbf{b}_{s2}$) are the corresponding reciprocal lattice vectors. (b) Folding mechanism and procedure from Z onto Z_s. (c) Step-by-step constructing process and (d) the final dispersion relation of the lattice based on the unit cell C_s (Inset: double Dirac cone at the 1st BZ center).

Distinct from the electrons of spin-1/2 [36,37], the key to realize the analogue of QSHE in spin-1 classical acoustic wave is to increase the degrees of freedom to twofold states to mimic pseudospins and pseudospin-orbit couplings. Consequently, fourfold degenerated double Dirac cones in the acoustic band structure are required. Here, we use the dispersion analysis of band folding [38] to get the double Dirac cones from the original honeycomb lattice, and propose the application possibilities in topological acoustics.

Let us start with the regular honeycomb acoustic metamaterial lattice [39–42]. Figure 1(a) shows the schematic of the honeycomb lattice of artificial "atoms" (blue cylinders) embedded in an air matrix. The artificial atoms on a deeply subwavelength scale r can be modeled by soft resonant scatterers with refractive index $n_m > n_A$, which can be achieved by using the soft metamaterial structures [43,44]. Here, n_m and n_A are refractive indexes of cylinders and air, respectively. This crystalline structure is organized by periodically repeating the primitive cell C (orange dashed rhombus defined by vectors $\mathbf{a}_1$ and $\mathbf{a}_2$) containing two identical atoms. The distance between the adjacent atoms is $R = 1$ cm, and the radius and refractive index are $r = 0.360$ cm and $n_m = 3.421 n_A$. Note that n_m has a wide range of applicable refractive index other than $3.421 n_A$ (Supplemental Material [45] Sec. IV). The obtained dispersion [Fig. 1(b)] exhibits single Dirac cones at the 1st Brillouin zone (BZ) corners (Supplemental Material [45] Sec. V). This double degenerated band structure is created by the presence of two equivalent scatterers. We emphasize that although the single Dirac cones in acoustic systems were discussed previously in both square [53] and triangular [54] lattices, possible nontrivial topology in acoustics using the Dirac dispersions without applied angular momentum was not addressed.

We further construct double Dirac cones at the 1st BZ center. First, the honeycomb lattice is equivalent to a triangular lattice of artificial metamolecules containing six neighboring atoms. Figure 1(a) shows the 30°-rotated augmented unit cell C_s with the lattice vectors ($\mathbf{a}_{s1}$, $\mathbf{a}_{s2}$) and lattice constant $a = 3$ cm. Assuming the Cartesian axes aligned with $\mathbf{a}_{s1}$ and $\mathbf{a}_{s2}$, the 1st BZs corresponding to C and C_s are plotted in Fig. 2(a) for comparison. The 1st BZ of C_s (denoted by Z_s) is completely enclosed by that of C (denoted by Z). Therefore, we pay special attention to the effects of the cell rotation and reveal the change of the dispersion curves. Figure 2(b) shows the zone folding mechanism and detailed procedure from Z onto Z_s, respectively. We focus on the 1/12 of the zone due to the symmetry, and other parts can be folded accordingly. In order to map the single Dirac cone at M to Γ_s, we proceed in two steps: we first fold part 1 (MXM_s) onto part 2

(MX_sM_s) along the folding line AB, and then fold part 2 onto part 3 $(\Gamma_sX_sM_s)$ along the folding line CD. The dispersion curves follow the mapping relations

$$(X_s\Gamma + X_sM + XM)|_{inZ} = X_s\Gamma_s|_{inZ_s}$$
$$(\Gamma M_s + MM_s + MM_s)|_{inZ} = \Gamma_sM_s|_{inZ_s}$$
$$(M_sX_s + M_sX_s + M_sX)|_{inZ} = M_sX_s|_{inZ_s}. \quad (1)$$

The step-by-step constructing processes are illustrated in Fig. 2(c), and the resulting dispersion relation of C_s is shown in Fig. 2(d). Four branches with linear dispersion intersect at a fourfold degenerate point at Γ_s ($\mathbf{k} = 0$) with the frequency of $f = 5278$ Hz, forming a double Dirac cone [inset of Fig. 2(d)] (Supplemental Material [45] Sec. V).

Owing to the linear dispersion of the Dirac cone, most of the progress in this area opens a topologically nontrivial band gap by breaking the time-reversal symmetry. Contrarily, with inherent time reversal invariants, we proceed to open nontrivial band gaps and produce edge states by lifting the degeneracy associated with double Dirac cone. Two new configurations have been created by breaking the lattice symmetry in opposite ways: (i) *contracting* the metamolecule by concentrating the six elements or (ii) *expanding* the metamolecule by distracting the elements. For both configurations, the distance R between the hexagonal packed scatterers and metamolecules' center deviates from $a/3$ (C_6 symmetric case). The dispersion relations for the triangular acoustic metamaterial lattice composed of contracting metamolecules with $R/a = 0.320$ and expanding metamolecules with $R/a = 0.345$ are illustrated in Fig. 3(a).

Two remarks should be noted. (i) Owing to the broken symmetry of the lattice, these fourfold degenerate acoustic states should split into two twofold degenerate states and open a bulk band gap. The pressure field distributions created by the metamolecules (the new element of the symmetry-broken system) are investigated carefully [Fig. 3(b)], and the following observation can be made: a multiple scattering inside the metamolecule creates a pair of dipolar resonant states accompanied by a pair of quadrupolar resonant states. The dipoles are even or odd symmetrical to the axes x/y (corresponding to p_x/p_y), while the quadrupole is odd symmetrical to the axes x and y (corresponding to d_{xy}), or even symmetrical to the axes x and y at the same time (corresponding to $d_{x^2-y^2}$). The angular momenta of the wave function of pressure fields $p_\pm = (p_x \pm ip_y)/\sqrt{2}$ and $d_\pm = (d_{x^2-y^2} \pm id_{xy})/\sqrt{2}$ further constitute the pseudospin in the present acoustic crystals [40,55].

We emphasize that the important thing here is to find the acoustic pseudospin multipolar states in the structure. In order to grasp the intrinsic physics of the pseudospin multipolar states, we check the real-space distributions of the pseudospin root-mean-square intensity $I = (1/T)\int_0^T \mathrm{Re}(p)\mathrm{Re}(v)dt$ with $T = 2\pi/\omega$, which describes the energy flow in the metamolecule. For simplicity, only the states below the band gap are illustrated in Figs. 3(c)–3(d). Intensity circulation around the metamolecule center and the chirality of the intensity corresponding to the pseudospin down and pseudospin up are clearly demonstrated (Supplemental Material [45], movie 1). We stress that these acoustic pseudospin multipolar states result from multiple scattering, without introducing a circulating fluid flow or ring waveguides. The artificial multipoles can exhibit distinct behavior with respect to the previous regular spinless reports (Supplemental Material [45] Sec. VI and movie 2) and offer promising novel applications.

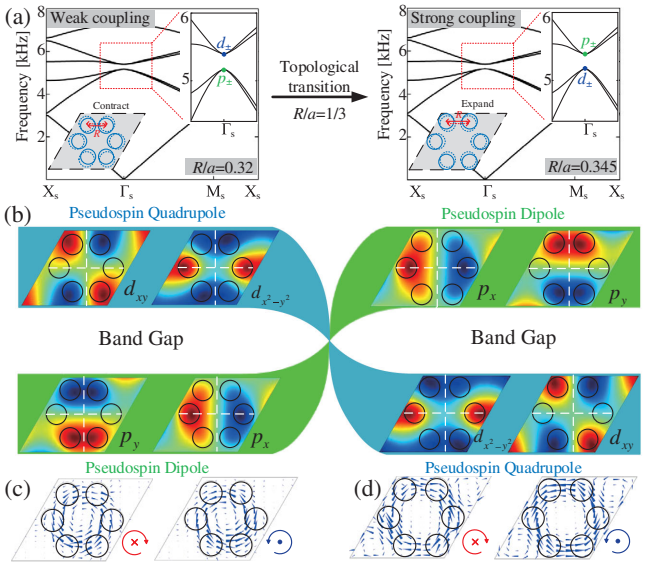

FIG. 3. (a) Topological transition as the coupling strength is tuned from weak (left: $R/a = 0.320$) to strong (right: $R/a = 0.345$). Critical coupling appears at $R/a = 1/3$ [Fig. 2(d)] with double Dirac cone. (b) Topological modes inversion underlying the transition. p_x and p_y show pseudospin dipole modes, while d_{xy} and $d_{x^2-y^2}$ show pseudospin quadrupole modes. Sound intensity I associated with pseudospin-down and pseudospin-up modes at the Γ_s point below the band gap in the (c) trivial regime ($R/a = 0.320$) and (d) nontrivial regime ($R/a = 0.345$). The rainbow color represents the amplitude of acoustic pressure, and the arrows show the direction and amplitude of the intensity.

(ii) Band inversion takes place upon increasing the ratio R/a in the symmetry-broken system (Supplemental Material [45], Secs. I–III and VII–VIII). When $R/a < 1/3$, the eigenstates bound to the bulk band gap have the normal band order [Fig. 3(b), left]: the lower-band-edge states have a pair of dipole states (in p-like symmetry), while the upper-band-edge states have a pair of quadrupole states (in d-like symmetry). This phenomenon is consistent with the classic acoustic theory, in which the dipole states must exhibit lower frequency than the higher-order quadrupole states. For $R/a > 1/3$, however, the dipole states rise above the quadrupole states, leading to an inverted band structure [Fig. 3(b), right]. This band inversion effect can be understood simply in the approximation that the system has inverted symmetry breaking. Although the contracting and

expanding metamolecules have the identical lattice constant a, the coupling strength between the adjacent metamolecules depends on the separation R (Supplemental Material [45], Sec. IX). Therefore, increasing R strengthens the pseudospin–orbit coupling. For a contracting configuration such as $R/a = 0.320$, the coupling effect is so weak that the cross talk between the pseudospin metamolecules is negligible [Fig. 3(c)] and the bands have a normal ordering. The acoustic energy flows around individual atoms only, characterizing a conventional "insulating" state. In certain expanding configuration such as $R/a = 0.345$, however, the pseudospin-orbit coupling is so strong [Fig. 3(d)] that the intensity is much enhanced in interstitial regimes and the dipole states are pushed above the quadrupole states band—that is, the bands are inverted. This phenomenon is analogous to the inverted conduction band and valence band by strong spin-orbit coupling in electronic topological insulators. Therefore, we achieve a topological phase transition by tuning the coupling strength between adjacent metamolecules (Supplemental Material [45], movie 3). Considering the generality in practical systems, we demonstrate that the topological creation is based on the band inversion between the pseudospin dipole (in p-like symmetry) and quadrupole (in d-like symmetry), which can be also obtained for different combinations, such as solid-in-air, solid-in-fluid, and air-in-fluid acoustic systems (Supplemental Material [45], Secs. X and XI). We also discuss symmetry broken by rotating the metamolecule without band inversion (Supplemental Material [45], Sec. XII).

One of the key manifestations of acoustic topological insulator is the pseudospin-dependent one-way transmission of sound edge states localized at the interface while being excluded from the bulk. Figure 4(b) shows the band structure of a ribbon-shaped supercell [Fig. 4(a)]. Here we clad the lower and upper edges of the topologically nontrivial region in terms of two trivial regions, which prevents possible edge states from leaking into free space. A bulk band gap can be found in the range from 5149 to 5351 Hz. The band gap is spanned by additional topological edge states as indicated by the double degenerated curves, which correspond to two sets of edge states confined to opposite edges of the ribbon, and which have opposite group velocities.

Figure 4(c) shows the real-space distributions of the pressure field at typical momenta around the Γ_s point [labeled as A and B in Fig. 4(b) with $k_{\|} = \pm 0.035 \times 2\pi/a$]. Two pairs of in-gap edge states are confined at the lower and upper edges and decay exponentially into bulk. The intensity exhibits a nonzero anticlockwise (clockwise) acoustic energy flow for the pseudospin-up (pseudospin-down) state even averaged over time. Thus, four spatially separated transmission channels are found: the upper edge contains a forward channel with pseudospin down and a backward channel with pseudospin up, and conversely for the lower edge. Note that the transmission channels for sound are split in a time-reversal-invariant fashion, without

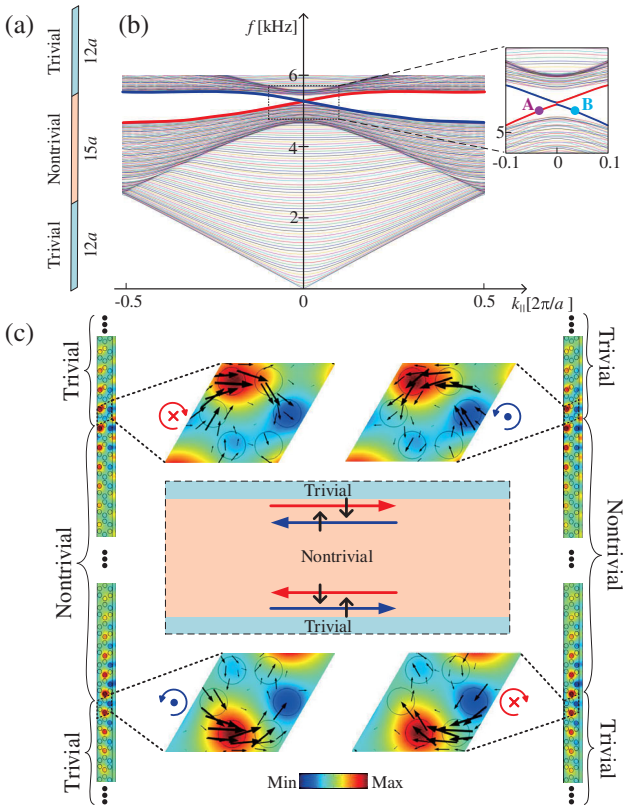

FIG. 4. (a) Schematic of a ribbon-shaped supercell composed of 15 and 24 metamolecules for the topologically nontrivial and trivial regions respectively. (b) Topological edge modes shown by the thick curves. (c) Acoustic pressure fields and intensity of the pseudospin-dependent one-way edge modes localized at the interface of the supercell, corresponding to the points A and B indicated in (b).

any background flow, as illustrated in the inset of Fig. 4(c) by the symbolic equation "$4 = 2 + 2$." This indicates unambiguously counterpropagations of acoustic energy at the sample edge associated with the two pseudospin states, the hallmark of a QSHE state. Consequently, when an acoustic pseudospin multipole encounters a scatterer, it can take either a clockwise or an anticlockwise turn with reversed pseudospin and perfect destructive interference, which leads to perfect transmission.

As the final example, we study the topological edge state in a finite $30a \times 39a$ lattice. As shown in top panels of Figs. 5(a) and 5(b), the gray trivial region encircles the blue nontrivial region of $15a \times 15a$. First, we excite pseudospin-down modes at the frequency of $f = 5233$ Hz from the lower end of the structure, and the incident sound cannot transmit along the edge [Fig. 5(a)]. Second, the same pseudospin mode is excited at the top edge [Fig. 5(b), top]. This produces a mode which propagates along the edge without obvious backscattering (Supplemental Material [45], Sec. XIII), including around two sharp corners of the lattice [Fig. 5(b), bottom]. Sound waves are localized in the vicinity of the edge and decay exponentially into bulk,

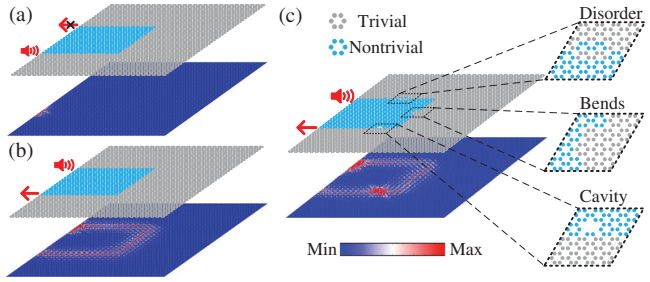

FIG. 5. Topologically protected one-way edge waveguide for airborne sound and the robustness against defects. The pseudospin-down mode is excited at the (a) lower and (b) upper edge. (c) Topological edge states with three kinds of defects: disorder, bends, and cavity. Bottom panels: the corresponding distributions of acoustic intensity fields.

indicating that the bulk region is insulating (Supplemental Material [45] Sec. XIV). We verify that the pseudospin-down sound can only propagate clockwise. However, this one-way transmission can be inversed by moving the atoms inside each metamolecule inward or outward to reconfigure the lattice (Supplemental Material [45] Sec. XV). The two pseudospin states will not affect each other at the same frequency and between different frequencies (Supplemental Material [45] Sec. XVI).

In order to confirm the topological robustness of the acoustic edge modes, we deliberately introduce three types of defects and investigate their influences [Fig. 5(c)]. These results confirm unambiguously that the sound transport is immune to backscattering by circumambulating around the disordered region or reorganizing the field distributions in the local defects. What is worth noting is that the pseudospin modes will not change after encountering the local defects (Supplemental Material [45] Sec. XVII). It is therefore evident that the supported edge mode is robust even if a variety of defects exist, which is a universal characteristic caused by the intrinsic topological feature of the acoustic topological insulators and its enabled topological protection. Compared with the ordinary waveguide, one-way sound transmission by means of pseudospin edge states is fundamentally insensitive to backscattering from arbitrarily shaped defects. This behavior is a distinguishing feature of the present topological waveguide (Supplemental Material [45] Sec. XVIII).

In conclusion, we have demonstrated the acoustic pseudospin multipoles and robust propagation of acoustic edge states in a flow-free symmetry-broken metamaterial lattice. The topological properties originate from the topological phase transition induced by the band inversion effect. Such a platform achieves a noticeable topological gap opening solely because of multiple scattering of waves off the scatterers, which requires neither fast fluid rotation nor preset ring waveguides with closed geometry. This behavior opens up new possibilities for transmitting sound waves along any desired path without back reflection and for implementing unique device functionalities.

This work was supported by the National Basic Research Program of China (2012CB921504), NSFC (11674172, 11574148, 11474162 and 11274171), SRFDP (2013009 1130004), and Jiangsu Provincial NSF (BK20160018 and BK20150562).

*chengying@nju.edu.cn
†liuxiaojun@nju.edu.cn

[1] K. Vonklitzing, G. Dorda, and M. Pepper, Phys. Rev. Lett. **45**, 494 (1980).
[2] R. B. Laughlin, Phys. Rev. Lett. **50**, 1395 (1983).
[3] C. L. Kane and E. J. Mele, Phys. Rev. Lett. **95**, 226801 (2005).
[4] B. A. Bernevig, T. L. Hughes, and S.-C. Zhang, Science **314**, 1757 (2006).
[5] M. Z. Hasan and C. L. Kane, Rev. Mod. Phys. **82**, 3045 (2010).
[6] D. Hsieh, D. Qian, L. Wray, Y. Xia, Y. S. Hor, R. J. Cava, and M. Z. Hasan, Nature (London) **452**, 970 (2008).
[7] R. Yu, W. Zhang, H.-J. Zhang, S.-C. Zhang, X. Dai, and Z. Fang, Science **329**, 61 (2010).
[8] X.-L. Qi and S.-C. Zhang, Rev. Mod. Phys. **83**, 1057 (2011).
[9] C. Nayak, S. H. Simon, A. Stern, M. Freedman, and S. Das Sarma, Rev. Mod. Phys. **80**, 1083 (2008).
[10] V. Peano, C. Brendel, M. Schmidt, and F. Marquardt, Phys. Rev. X **5**, 031011 (2015).
[11] W. Gao, M. Lawrence, B. Yang, F. Liu, F. Fang, B. Béri, J. Li, and S. Zhang, Phys. Rev. Lett. **114**, 037402 (2015).
[12] S. Xiao, F. Zhong, H. Liu, S. Zhu, and J. Li, Nat. Commun. **6**, 8360 (2015).
[13] L. M. Nash, D. Kleckner, A. Read, V. Vitelli, A. M. Turner, and W. T. M. Irvine, Proc. Natl. Acad. Sci. U.S.A. **112**, 14495 (2015).
[14] R. Suesstrunk and S. D. Huber, Science **349**, 47 (2015).
[15] R. Susstrunk and S. D. Huber, Proc. Natl. Acad. Sci. U.S.A. **113**, E4767 (2016).
[16] F. D. M. Haldane and S. Raghu, Phys. Rev. Lett. **100**, 013904 (2008).
[17] Z. Wang, Y. D. Chong, J. D. Joannopoulos, and M. Soljacic, Phys. Rev. Lett. **100**, 013905 (2008).
[18] Z. Wang, Y. Chong, J. D. Joannopoulos, and M. Soljacic, Nature (London) **461**, 772 (2009).
[19] K. Fang, Z. Yu, and S. Fan, Nat. Photonics **6**, 782 (2012).
[20] A. B. Khanikaev, S. Hossein Mousavi, W.-K. Tse, M. Kargarian, A. H. MacDonald, and G. Shvets, Nat. Mater. **12**, 233 (2013).
[21] T. Ma, A. B. Khanikaev, S. H. Mousavi, and G. Shvets, Phys. Rev. Lett. **114**, 127401 (2015).
[22] G. Q. Liang and Y. D. Chong, Phys. Rev. Lett. **110**, 203904 (2013).
[23] M. Hafezi, E. A. Demler, M. D. Lukin, and J. M. Taylor, Nat. Phys. **7**, 907 (2011).
[24] M. Hafezi, S. Mittal, J. Fan, A. Migdall, and J. M. Taylor, Nat. Photonics **7**, 1001 (2013).
[25] R. Fleury, A. B. Khanikaev, and A. Alu, Nat. Commun. **7**, 11744 (2016).
[26] A. B. Khanikaev, R. Fleury, S. H. Mousavi, and A. Alu, Nat. Commun. **6**, 8260 (2015).

[27] Z. Yang, F. Gao, X. Shi, X. Lin, Z. Gao, Y. Chong, and B. Zhang, Phys. Rev. Lett. **114**, 114301 (2015).
[28] R. Fleury, D. L. Sounas, C. F. Sieck, M. R. Haberman, and A. Alù, Science **343**, 516 (2014).
[29] C. He, Z. Li, X. Ni, X.-C. Sun, S.-Y. Yu, M.-H. Lu, X.-P. Liu, and Y.-F. Chen, Appl. Phys. Lett. **108**, 031904 (2016).
[30] S. H. Mousavi, A. B. Khanikaev, and Z. Wang, Nat. Commun. **6**, 8682 (2015).
[31] Z.-G. Chen and Y. Wu, Phys. Rev. Applied **5**, 054021 (2016).
[32] X. Ni, C. He, X. C. Sun, X. P. Liu, M. H. Lu, L. Feng, and Y. F. Chen, New J. Phys. **17**, 053016 (2015).
[33] C. Shen, Y. Xie, N. Sui, W. Wang, S. A. Cummer, and Y. Jing, Phys. Rev. Lett. **115**, 254301 (2015).
[34] M. Xiao, G. Ma, Z. Yang, P. Sheng, Z. Q. Zhang, and C. T. Chan, Nat. Phys. **11**, 240 (2015).
[35] P. Dziawa *et al.*, Nat. Mater. **11**, 1023 (2012).
[36] O. Leenaerts, B. Partoens, and F. M. Peeters, Appl. Phys. Lett. **103**, 013105 (2013).
[37] J. Feng, L. Qi, J. Y. Huang, and J. Li, Phys. Rev. B **80**, 165407 (2009).
[38] Y. K. Ahn, J. H. Oh, P. S. Ma, and Y. Y. Kim, Wave Motion **61**, 63 (2016).
[39] M. Xiao, W.-J. Chen, W.-Y. He, and C. T. Chan, Nat. Phys. **11**, 920 (2015).
[40] L.-H. Wu and X. Hu, Phys. Rev. Lett. **114**, 223901 (2015).
[41] D. Torrent and J. Sánchez-Dehesa, Phys. Rev. Lett. **108**, 174301 (2012).
[42] D. Torrent, D. Mayou, and J. Sánchez-Dehesa, Phys. Rev. B **87**, 115143 (2013).
[43] M. D. Guild, V. M. García-Chocano, J. Sánchez-Dehesa, T. P. Martin, D. C. Calvo, and G. J. Orris, Phys. Rev. Applied **5**, 034012 (2016).
[44] Y. Cheng, C. Zhou, B. G. Yuan, D. J. Wu, Q. Wei, and X. J. Liu, Nat. Mater. **14**, 1013 (2015).
[45] See Supplemental Material at http://link.aps.org/supplemental/10.1103/PhysRevLett.118.084303, which includes Refs. [46–52], for the discussion of the $k \cdot P$ model in acoustic lattice, comparison between topological edge states and transmission states, reconfigurable topological one-way transmission, the generality of the topological insulator in practical systems, the interaction between different pseudospin states, coupling strength between the adjacent metamolecules, comparison between the topological waveguide and ordinary waveguide, pseudospin states when encountering the local disorder and defects, and tightness of the edge states.
[46] J. Mei, Y. Wu, C. T. Chan, and Z.-Q. Zhang, Phys. Rev. B **86**, 035141 (2012).
[47] S.-Q. Shen, W.-Y. Shan, and H.-Z. Lu, SPIN **01**, 33 (2011).
[48] T. Brunet, J. Leng, and O. Mondain-Monval, Science **342**, 323 (2013).
[49] B. Liang, X. S. Guo, J. Tu, D. Zhang, and J. C. Cheng, Nat. Mater. **9**, 989 (2010).
[50] M. Lanoy, R. Pierrat, F. Lemoult, M. Fink, V. Leroy, and A. Tourin, Phys. Rev. B **91**, 224202 (2015).
[51] A. Bretagne, A. Tourin, and V. Leroy, Appl. Phys. Lett. **99**, 221906 (2011).
[52] V. Leroy, A. Bretagne, M. Fink, H. Willaime, P. Tabeling, and A. Tourin, Appl. Phys. Lett. **95**, 171904 (2009).
[53] X. Huang, Y. Lai, Z. H. Hang, H. Zheng, and C. T. Chan, Nat. Mater. **10**, 582 (2011).
[54] J. Lu, C. Qiu, M. Ke, and Z. Liu, Phys. Rev. Lett. **116**, 093901 (2016).
[55] C. He, X. Ni, H. Ge, X.-C. Sun, Y.-B. Chen, M.-H. Lu, X.-P. Liu, and Y.-F. Chen, Nat. Phys. **12**, 1124 (2016).